

How to measure the Majorana polarization of a topological planar Josephson junction

Szczepan Głodzik ,^{*} Nicholas Sedlmayr ,[†] and Tadeusz Domański [‡]

Institute of Physics, M. Curie-Skłodowska University, 20-031 Lublin, Poland



(Received 11 April 2020; accepted 27 July 2020; published 7 August 2020)

We analyze the topological superconductivity and investigate the spectroscopic properties manifested by the zero-energy modes, induced in a metallic strip embedded into a Josephson-type junction. Focusing on the Majorana polarization of such quasiparticles, we propose feasible means for its empirical detection, using the spin-selective Andreev reflection method. Our study reveals a gradual development of a transverse gradient of the Majorana polarization across the metallic strip upon increasing its width. We also inspect the spatial profile and polarization of the Majorana quasiparticles in the presence of a strong electrostatic impurity. We show that, depending on its position, such a defect can lead to a substantial localization of the Majorana mode.

DOI: [10.1103/PhysRevB.102.085411](https://doi.org/10.1103/PhysRevB.102.085411)

I. INTRODUCTION

Topological materials, including those which are either insulators or superconductors, differ qualitatively from their ordinary counterparts due to the emergence of protected in-gap modes. Such quasiparticles, which develop at boundaries or internal defects, are topologically protected (thus being good candidates for stable qubits), and obey fractional statistics (which is appealing for quantum computations). Experimental efforts for the realization of these exotic quasiparticles have so far largely focused on one-dimensional structures, e.g., semiconducting nanowires proximitized to superconductors [1–5], nanochains of magnetic atoms deposited on superconducting substrates [6–11], and lithographically fabricated nanostructures [12]. Another direction in pursuit of topological superconductivity relies on two-dimensional systems, where the in-gap quasiparticles are chiral modes [13–17]. Such Majorana edge modes have indeed been observed in STM measurements, using nanoscopic islands of magnetic atoms deposited on superconducting substrates [18–20]. Further interesting perspectives are related with mixed-dimensionality systems, where the localized and delocalized Majorana quasiparticles coexist with one another [21,22]. In particular, nanowires attached to larger structures [12] could enable a controllable transfer of the Majorana modes between these constituents [23], probing their Chern numbers [24].

Yet another promising platform for the realization of topological superconductivity hosting the Majorana modes has been suggested in Refs. [25,26] using normal strips characterized by a strong spin-orbit coupling, embedded between two superconducting leads with differing phases (see Fig. 1). Signatures of the zero-energy modes have already been reported for such heterostructures, consisting of aluminum on indium arsenide [27] and an HgTe quantum well coupled to

a thin aluminum film [28]. The major virtue of a Josephson-type geometry is its tunability to the topologically nontrivial regime, that can be controlled experimentally by the phase difference. Another method for a controllable transition to the topological phase is possible by embedding two gate-tunable Josephson junctions in a phase-sensitive SQUID geometry, as reported for epitaxial Al/InAs heterostructures [29]. Experiments on these Josephson-junction heterostructures [27–29] have triggered further intensive studies [30–33]. The proximitized strips are hoped, for instance, to enable a current-controlled braiding of the Majorana modes [34]. It has also been suggested [35] that weak disorder might promote localization of the Majorana quasiparticles.

Topological superconductivity of the phase-controlled Josephson heterostructures has been observed spectroscopically in the narrow (albeit finite-width) normal strips placed between conventional superconductors. The group in Copenhagen used for this purpose a (1.6–5 μm long and 40–120 nm wide) InAs region [27], while in Harvard they explored (1–4 μm long and 400–600 nm wide) HgTe quantum wells [28]. In both cases, dimensionality might have played an important role, affecting the character of the boundary modes. A convenient tool to deal with this issue is the *Majorana polarization*, introduced in Ref. [36], which is capable to inspect and identify topological nature of the zero-energy quasiparticles [21,36–38].

Formally, the Majorana polarization is the local expectation value of the particle-hole operator for a given eigenstate [36]. It has been shown to be useful for calculating the topological phase diagram when alternative methods (specific either for one- or two-dimensional systems) cannot be adopted, and for recognizing whether the low-energy states are the true Majorana quasiparticles [21,36,37]. In the present context, the quasi-two-dimensionality of the proximitized strips is expected to induce transverse gradients in the Majorana polarization [39]. They would be observable in the phase of the Majorana polarization vector, and in its absolute value. Transverse gradients of the Majorana polarization, relative to the density, could be an indication of a delocalization process

^{*}szglodzik@kft.umcs.lublin.pl

[†]sedlmayr@umcs.pl

[‡]doman@kft.umcs.lublin.pl

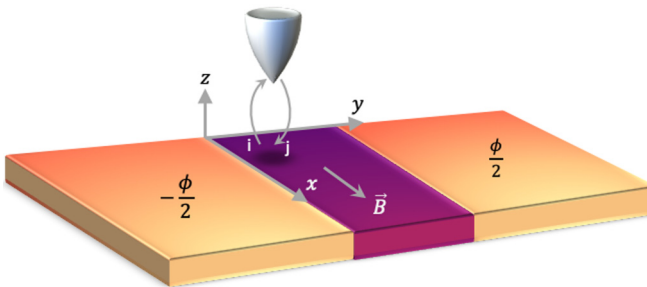


FIG. 1. A schematic view of a metallic strip (dark purple), embedded between superconducting regions (yellow) which differ in phase by ϕ , probed by a polarized STM tip (light gray). A magnetic field $\vec{B} = B_0 \hat{x}$ is applied to the whole structure.

that ultimately might be detrimental to the zero-energy modes. Details concerning the Majorana polarization are presented in Sec. III B.

Furthermore, we prove (in Sec. IV) that the modulus of the Majorana polarization would be accessible experimentally using selective equal spin Andreev reflection spectroscopy [40]. A similar technique has been already applied to detect the spin polarization of the Majorana quasiparticles of Fe atom chains deposited on superconducting Pb [10,38] and to probe the zero-energy mode confined in a vortex core of a two-dimensional Bi₂Te₃/NbSe₂ heterostructure [41]. The method proposed here could be an unambiguous probe of the Majorana nature of the zero-energy quasiparticles.

Finally, we address how robust the Majorana quasiparticles of the phase-controlled Josephson junctions are against an electrostatic scattering potential placed in various regions of the proximitized strip. Our study reveals that, when this local defect is placed in an interior of the strip, its influence on the Majorana modes is practically negligible, but when placed near a region of the existing Majorana quasiparticle we observe a tendency toward reducing the spatial extent of the zero-energy modes, analogous to what has been predicted by Haim and Stern in the disordered case [35]. These phenomena are in stark contrast to the properties of Majorana quasiparticles of strictly one-dimensional systems, where strong local defects usually produce additional pairs of the Majorana modes.

The paper is organized as follows. In Sec. II we present the microscopic model and outline methodological details. Next, in Sec. III, we inspect the spatial profiles of the zero-energy modes and consider their Majorana polarization, focusing on their evolution upon varying the width of the proximitized strip. Section IV presents the selective Andreev spectroscopy and shows that it can probe the modulus of the *symmetrized* Majorana polarization. Section V discusses the localization of the Majorana quasiparticle driven by a pointlike electrostatic defect, and Sec. VI summarizes the main results.

II. MICROSCOPIC MODEL

For a schematic of the planar Josephson heterostructure (see Fig. 1), here we employ the microscopic scenario discussed in Refs. [25,26,32]. The model tight-binding

Hamiltonian

$$\mathcal{H} = \mathcal{H}_0 + \mathcal{H}_Z + \mathcal{H}_S \quad (1)$$

consists first of the free term

$$\mathcal{H}_0 = \sum_{\langle i, j \rangle} [i\lambda(\mathbf{d}_{ij} \times \vec{\sigma}_{\sigma\sigma'})_z - t\delta_{\sigma\sigma'}] d_{i\sigma}^\dagger d_{j\sigma'} - \mu \sum_{i\sigma} d_{i\sigma}^\dagger d_{i\sigma} \quad (2)$$

describing itinerant electrons hopping all over the sample. t is the hopping integral between the nearest-neighbor atomic sites on a square lattice, λ is the strength of the Rashba spin-orbit coupling, \mathbf{d}_{ij} is the vector connecting nearest neighbors, and σ stands for the vector of the Pauli matrices. The second (Zeeman) term

$$\mathcal{H}_Z = B_0 \sum_i \sum_{\sigma\sigma'} d_{i\sigma}^\dagger \sigma_{\sigma\sigma'}^x d_{i\sigma'} \quad (3)$$

accounts for the influence of an external magnetic field B_0 which is parallel to the interface between the metallic and superconducting regions, as reported experimentally [27,28]. The last part appearing in the model Hamiltonian (1) describes the onsite pairing in the left (S_L) and right (S_R) superconducting regions,

$$\mathcal{H}_S = \sum_i (\Delta_i d_{i\downarrow}^\dagger d_{i\uparrow}^\dagger + \text{H.c.}), \quad (4)$$

where

$$\Delta_i = \begin{cases} \Delta e^{-i\phi/2} & \text{for } i \in S_L, \\ \Delta e^{i\phi/2} & \text{for } i \in S_R, \\ 0 & \text{for } i \in N. \end{cases} \quad (5)$$

Here the metallic strip region is denoted by N . The phase difference between the superconducting layers S_R and S_L is ϕ and Δ is real.

We studied the finite-size version of this model, consisting of N_x sites along the x direction and N_y sites along the y direction. For specific computations we assumed $N_x = 91$ and $N_y = 30$, unless stated otherwise. The eigenstates and eigenenergies of the heterostructure were determined numerically, solving the Bogoliubov-de Gennes equations with the canonical transformation

$$\begin{pmatrix} d_{i\uparrow} \\ d_{i\downarrow}^\dagger \end{pmatrix} = \sum_n \begin{pmatrix} u_{i\uparrow}^n & v_{i\uparrow}^n \\ -(v_{i\downarrow}^n)^* & (u_{i\downarrow}^n)^* \end{pmatrix} \begin{pmatrix} \gamma_n \\ \gamma_n^\dagger \end{pmatrix}, \quad (6)$$

where $\gamma_n^{(\dagger)}$ stand for the Bogoliubov quasiparticles which diagonalize the Hamiltonian: $H = \sum_n E_n \gamma_n^\dagger \gamma_n + \text{const.}$

III. TOPOGRAPHY OF THE MAJORANA MODES

Upon substituting the metallic strip between the superconducting reservoirs, their Cooper pairs leak into the normal region, inducing onsite electron pairing. This proximity effect is efficient nearby the bulk superconductors, up to distances smaller than the coherence length ξ . Here, we consider metallic samples comprising a few N_w atomic rows, whose spatial width $N_w a \leq \xi$, where a is the interatomic distance. Under such a condition the proximity effect induces superconductivity across the entire metallic region. A fully self-consistent

study of the pairing gap in all parts of this heterostructure has been discussed in Ref. [30].

The topological superconducting phase originates from the triplet pairing, which can be achieved by combining the onsite pairing with the spin-orbit Rashba interaction and Zeeman splitting [5]. It has been demonstrated [25,26,30–33] that a transition from the topologically trivial to the nontrivial superconducting state is sensitive to the Josephson phase ϕ . Characteristic features of the emerging Majorana quasiparticles can, however, additionally depend on the width $N_w a$ of the metallic strip. In what follows, we analyze such qualitative changes observable in the spectral function and the Majorana polarization vector. We also propose a method for empirical detection of the Majorana polarization (Sec. IV).

A. Zero-energy spectral function

Focusing on the optimal condition for the topological superconducting state $\phi = \pi$, we have checked that the onsite pairing $\langle d_{i\downarrow} d_{i\uparrow} \rangle$ spreads nearly uniformly onto the metallic strip, both along and across it. Furthermore, we also noticed some feedback of the metallic sector onto superconducting regions manifested by partial reduction of the local pairing, sometimes referred to as the inverse superconducting proximity effect.

In presence of the spin-orbit interaction and the Zeeman field, the proximitized strip develops intersite pairing of identical spin electrons, i.e., triplet pairing. For sufficiently strong magnetic fields B_0 , such a triplet superconducting phase becomes topologically nontrivial, leading to the emergence of the zero-energy quasiparticles [25,26]. Their signatures can be observed in the local density of states

$$\rho_i(\omega) = \sum_{n,\sigma} [|u_{i\sigma}^n|^2 \delta(\omega - E_n) + |v_{i\sigma}^n|^2 \delta(\omega + E_n)]. \quad (7)$$

As we consider a finite-size system we have broadened the delta peaks to Lorentzian functions of width 0.02Δ .

Figure 2 displays the spatial profiles of the local density of states at zero energy $\rho_i(0)$, obtained for very narrow metallic strips. We note that the Majorana quasiparticles of the narrow metallic strip are well localized at its ends. Their overall topography is practically identical with all features of one-dimensional systems, including the characteristic oscillations along the metallic strip [42]. It comes as perhaps some surprise that this narrow width of metallic region is neither essential for the development of the topological superconducting phase, nor important for the spatial profile of the Majorana modes. Even in the extreme case $N_w = 0$, i.e., without any metallic piece between the phase-differing superconductors, such modes are still present. On the other hand, when the width N_w increases we see a gradual smearing of the zero-energy quasiparticles. This is a consequence of the reduced proximity-induced gap in wider strips which naturally reduces the localization of any mid-gap states.

B. Majorana polarization

Majorana modes are quasiparticles with energy $E_n = 0$ (we denote such doubly degenerate eigenstates by $n \equiv n_0$) and which are eigenstates of the particle-hole transformation

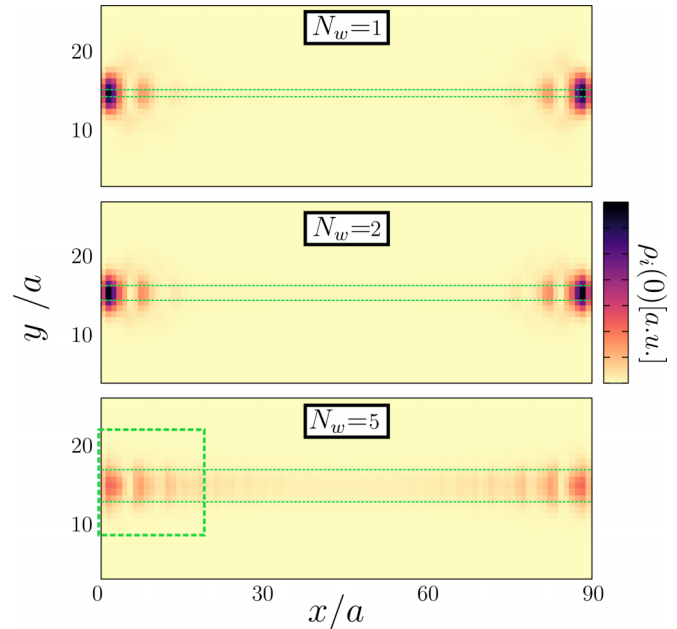


FIG. 2. The spatial profiles $\rho_i(0)$ of the Majorana quasiparticles appearing in a metallic strip consisting of 1, 2, and 5 rows of atomic chains, as indicated. We have used the model parameters $\Delta = 0.25t$, $\phi = \pi$, $\lambda = 0.5t$, $B_0 = 0.1t$, $\mu = -3.75t$. The Majorana polarization (10) for the area in the green square is shown in Fig. 3.

operator. We analyze here another valuable source of information about these modes encoded in the Majorana polarization [36,37,43,44]. This quantity is particularly useful for characterizing the Majorana modes of quasi-two-dimensional topological superconductors [21,36,39] where its phase develops both longitudinal and transverse variation. As we shall see, its texture brings an important message about the delocalized Majorana quasiparticles.

Formally, the particle-hole overlap can be defined for any eigenstate $|\psi_n\rangle$ [21,36]:

$$\mathcal{P}_{in} = \langle \psi_n | \mathcal{C} \hat{r}_i | \psi_n \rangle = \sum_{\sigma} \sigma_{\sigma\sigma}^z 2 u_{i\sigma}^n v_{i\sigma}^n, \quad (8)$$

where \hat{r}_i is projection onto site i and \mathcal{C} is the particle-hole operator. More generally, one may wish to consider the particle-hole overlap $u_{i\sigma_1}^n v_{j\sigma_2}^m$. In particular, the equal-spin pairing ($\sigma_1 = \sigma_2$) induced between the neighboring sites i and j for the zero-energy quasiparticles ($E_n = 0 = E_m$) would be of our interest here. For convenience we introduce the local Majorana polarization

$$\mathcal{P}_i = \mathcal{P}_{i\uparrow} - \mathcal{P}_{i\downarrow}, \quad (9)$$

where

$$\mathcal{P}_{i\sigma} = 2 u_{i\sigma}^{n_0} v_{i\sigma}^{n_0}. \quad (10)$$

This complex quantity (9) allows one to probe the Majorana eigenstates $E_{n_0} = 0$.

Let us start by checking the contributions $\mathcal{P}_{i\sigma}$ from each spin σ to the Majorana polarization in the narrow metallic strips, when the zero-energy quasiparticles are well localized near its ends. To be specific, we focus on the region marked by the dashed lines in the bottom panel in Fig. 2. Both

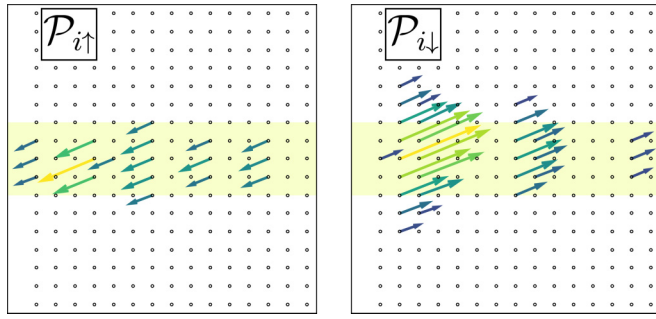


FIG. 3. Components of the Majorana polarization $\mathcal{P}_{i\sigma}$ obtained for the region highlighted by the dashed frame in Fig. 2. The magnitude of the arrows shows $|\mathcal{P}_{i\sigma}|$ and their direction shows $\text{Arg } \mathcal{P}_{i\sigma}$. We note that the phase of the Majorana polarization is only well defined up to a global shift. The shaded region is the metallic strip.

constituents $\mathcal{P}_{i\sigma}$ are depicted in Fig. 3 on the lattice sites of the marked metallic region. We clearly note that the directions of the arrows depicting $\mathcal{P}_{i\uparrow}$ are opposite to $\mathcal{P}_{i\downarrow}$, which is typical for strictly one-dimensional topological superconductors (see Fig. 2 in Ref. [38]) and for higher dimensions as well [21,36,39]. The magnitudes of the two components, shown by the length of the arrows, are however very different. It is important to emphasize that for the realization of a true Majorana bound state (MBS) the local phase of $\mathcal{P}_{i\uparrow} - \mathcal{P}_{i\downarrow}$ must be constant. Such a constraint $\mathcal{P}_{i\uparrow} = e^{i\varphi} |\mathcal{P}_{i\uparrow}| = -e^{i\varphi} |\mathcal{P}_{i\downarrow}|$ seems to be satisfied in our case only for narrow metallic strips.

There are in fact two conditions on \mathcal{P}_i which are required for Majorana modes. The first, which we have seen here, is that its phase must be constant. The phase of \mathcal{P}_i does not appear to be measurable in any simple way. What is measurable, as we will show in Sec. IV, is its modulus $|\mathcal{P}_i|$. For a Majorana mode we require $|\mathcal{P}_i| = \rho_i^0$, and this gives a measurable determination of Majorana modes. Upon increas-

ing the width of the metallic strip the Majorana polarization gradually develops varying orientations, both along and across the sample. Emergence of the transverse gradient is very sensitive to the width N_w , as illustrated in Fig. 4. We thus observe that the Majorana polarization vector has more subtle structure in comparison to the spectral function $\rho_i(0)$. In the next section we shall discuss empirical means to probe this quantity.

IV. POLARIZED ANDREEV SPECTROSCOPY

Here, we discuss an empirical method based on spin-polarized Andreev reflection spectroscopy [40], which could probe the absolute value of the Majorana polarization. Let us consider a scanning tunneling microscope (STM) tip brought in contact with site j of our heterostructure. The influence of this external reservoir of itinerant electrons can be incorporated by augmenting the model Hamiltonian (1) with the local term

$$H_j = \underbrace{\sum_{\mathbf{k},\sigma} (\varepsilon_{\mathbf{k}} - \mu_{\text{tip}}) c_{\mathbf{k}\sigma}^\dagger c_{\mathbf{k}\sigma} + \text{H.c.}}_{\text{STM tip}} + \underbrace{\sum_{\mathbf{k},\sigma} (t_{\mathbf{k},\sigma} c_{\mathbf{k}\sigma}^\dagger d_{j\sigma} + \text{H.c.})}_{\text{hybridization}}, \quad (11)$$

where the chemical potential of the tip $\mu_{\text{tip}} = \mu + eV$ can be varied by a bias potential V . $\varepsilon_{\mathbf{k}}$ is the dispersion of the tip electrons and $t_{\mathbf{k},\sigma}$ denotes the tunneling amplitude from the tip to the heterostructure and vice versa. The quasiparticle spectrum at site j can be indirectly inferred from measurements of the charge transport induced by the voltage V applied between the STM tip and the sample. In the subgap regime, i.e., for $e|V| \leq \Delta$, the sole contribution to such a current is from Andreev scattering processes. This mechanism relies on the conversion of electrons arriving from the STM tip into the Cooper pairs of the superconducting heterostructure, reflecting holes back into the STM tip.

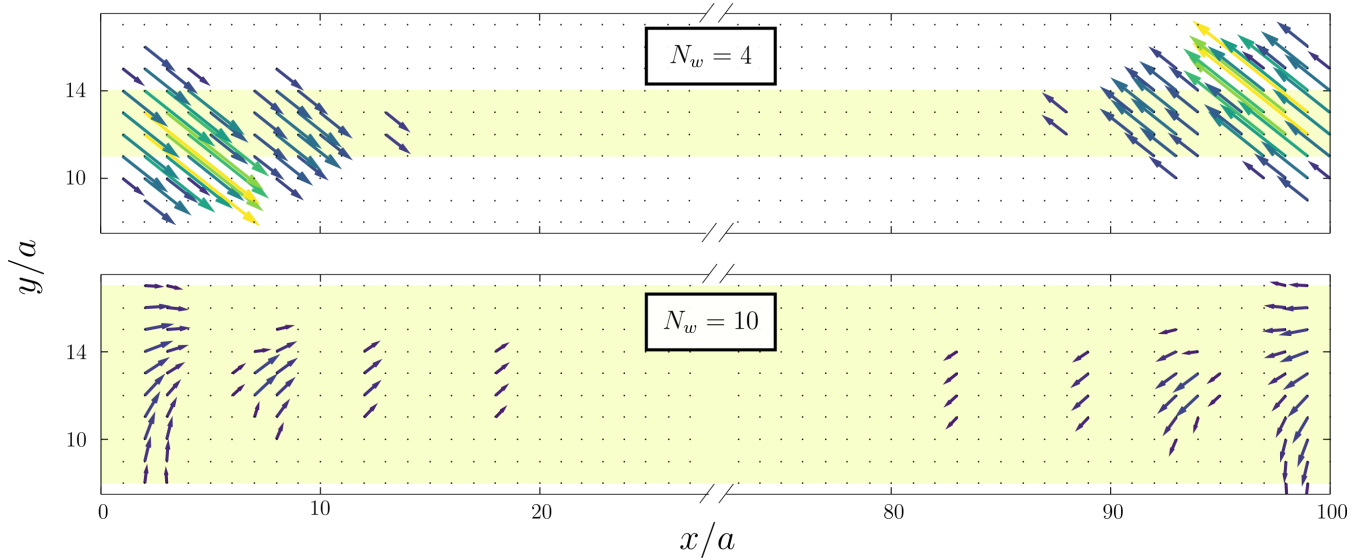


FIG. 4. The Majorana polarization \mathcal{P}_i obtained for the heterostructure comprising $N_w = 4$ (top) and $N_w = 10$ (bottom) atomic rows in the metallic strip, marked by the shaded region. Numerical results are obtained for the same model parameters as in Fig. 2 but using $N_x = 100$, $N_y = 20$. The magnitude of the arrows shows $|\mathcal{P}_{i\sigma}|$ and their direction shows $\text{Arg } \mathcal{P}_{i\sigma}$. We note that the phase is only well defined up to a global shift.

Since we are interested in probing the topological superconducting phase related to the intersite pairing of identical spin electrons, similar to the Kitaev scenario [45], let us assume a complete polarization of the tip electrons. Under such circumstances, only one spin component participates in the charge transport. On a microscopic level we can thus imagine an electron of spin σ arriving from the polarized STM tip at site j , where it forms the triplet pair with another electron of the same spin from the neighboring site i , reflecting a hole back into the tip.

The charge flow from the STM tip can be defined as $I^\sigma(V) = -e\langle \frac{d}{dt} \sum_{\mathbf{k}} c_{\mathbf{k}\sigma}^\dagger c_{\mathbf{k}\sigma} \rangle$. Using the Heisenberg equation of motion we can recast it in terms of the lesser Green's function $I^\sigma(V) = \frac{2e}{\hbar} \sum_{\mathbf{k}} \text{Re}\{\langle d_{j\sigma}; c_{\mathbf{k},\sigma}^\dagger \rangle\}$ whose determination is feasible within the Keldysh approach. Let us remark, however, that due to the intersite (triplet) pairing the operator $d_{j\sigma}$ would be coupled to the neighboring site operator $d_{i\sigma}$. For this reason such a current originating from Andreev scattering through the sites j and i (as illustrated in Fig. 1) will be explicitly denoted by subindices $I_{ij}^\sigma(V) \equiv I_{ij}^\sigma(V)$.

Following the steps, outlined previously by one of us in Ref. [38], the spin-polarized Andreev current can be expressed by the popular Landauer-type formula

$$I_{ij}^\sigma(V) = \frac{e}{h} \int d\omega T_{ij}^\sigma(\omega) [f(\omega - eV) - f(\omega + eV)], \quad (12)$$

where $f(\omega) = [1 + \exp(\omega/k_B T)]^{-1}$ is the Fermi-Dirac distribution function. The main quantities of our interest would be the spatially dependent transmission probabilities, characterizing conversion of electrons into holes on the neighboring sites [38]

$$T_{ij}^\sigma(\omega) = \Gamma_N^2 |\mathcal{F}_{ij}^\sigma(\omega)|^2, \quad (13)$$

where $\mathcal{F}_{ij}^\sigma(\omega) = \langle\langle \hat{d}_{i\sigma}; \hat{d}_{j\sigma} \rangle\rangle_\omega$ is the Fourier transform of the off-diagonal (in Nambu representation) retarded Green's function. For practical reasons (since we focus on a narrow transport window being a fraction of meV around the chemical potential μ) we have introduced a constant coupling strength $\Gamma_N \equiv 2\pi \sum_{\mathbf{k}} |\gamma_{\mathbf{k}}|^2 \delta(\omega - \varepsilon_{\mathbf{k}})$. Formally, this is equivalent to the wide-band-limit approximation.

In the absence of the STM tip the Green's function $\mathcal{F}_{ij}^\sigma(\omega)$ can be found explicitly from the Bogoliubov-de Gennes diagonalization (6). In particular, for $\sigma = \uparrow$ the transformation $d_{i\uparrow} = \sum_n [u_{i\uparrow}^n \gamma_n + v_{i\uparrow}^n \gamma_n^\dagger]$ implies

$$\lim_{\mathbf{k}, \sigma=0} \langle\langle d_{i\uparrow}; d_{j\uparrow} \rangle\rangle_\omega = \sum_n \left[\frac{u_{i\uparrow}^n v_{j\uparrow}^n}{\omega - E_n} + \frac{v_{i\uparrow}^n u_{j\uparrow}^n}{\omega + E_n} \right] \quad (14)$$

and a similar expression (with minus sign) holds for $\sigma = \downarrow$. The effect of the hybridization term introduced in Eq. (11) can be modeled in the wide-band-limit approximation by the substitution $\omega \rightarrow \omega + i\frac{\Gamma_N}{2}$ (see Appendix A in Ref. [46] for a detailed derivation). Physically, it means that the STM tip gives rise to a broadening of the subgap quasiparticles, i.e., to a finite lifetime. The Green's function $\mathcal{F}_{ij}^\sigma(\omega)$ is thus given by

$$\mathcal{F}_{ij}^\sigma(\omega) = \sum_n \left[\frac{u_{i\uparrow}^n v_{j\uparrow}^n}{\omega - E_n + i\frac{\Gamma_N}{2}} + \frac{u_{j\uparrow}^n v_{i\uparrow}^n}{\omega + E_n + i\frac{\Gamma_N}{2}} \right], \quad (15)$$

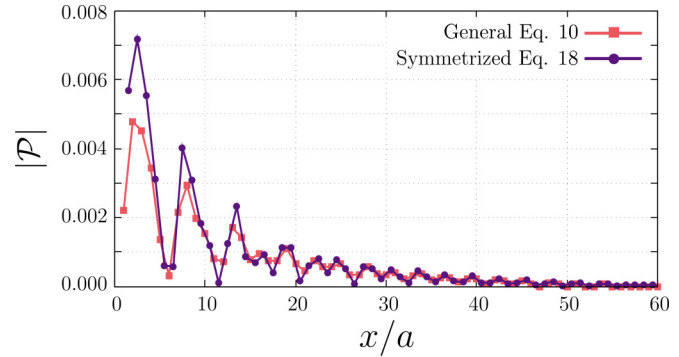


FIG. 5. Comparison of the Majorana polarization (9) with its symmetrized version defined in Eq. (18) computed for the central row of the metallic strip using $N_w = 5$ and the same model parameters as presented in Fig. 6.

where the complex coefficients $u_{j\uparrow}^n$ and $v_{j\uparrow}^n$ have to be obtained numerically from the diagonalization procedure.

Focusing on the zero-energy limit $\omega \rightarrow 0$, dominated by the Andreev scatterings via the Majorana quasiparticle (denoted here by $E_{n_0} = 0$), we obtain the transmittance (13) simplified to

$$T_{ij}^\sigma(\omega = 0) \simeq |2u_{io}^{n_0} v_{j\sigma}^{n_0} + 2u_{j\sigma}^{n_0} v_{io}^{n_0}|^2. \quad (16)$$

Equation (16) substituted into the spin-resolved Andreev current formula (12) yields, at low temperatures, the following zero-bias differential conductance:

$$\lim_{V \rightarrow 0} \frac{dI_{ij}^\sigma(V)}{dV} \simeq \frac{4e^2}{h} |u_{io}^{n_0} v_{j\sigma}^{n_0} + u_{j\sigma}^{n_0} v_{io}^{n_0}|^2. \quad (17)$$

This result demonstrates that the polarized Andreev spectroscopy could probe the spin-dependent contribution (10) to the Majorana polarization. Strictly speaking, however, such tunneling processes occur on the links (involving the neighboring sites j and i) rather than on individual local sites. For this reason the differential conductance (17) would measure the *symmetrized Majorana polarization*

$$\mathcal{P}_{(ij),\sigma} = u_{io}^{n_0} v_{j\sigma}^{n_0} + u_{j\sigma}^{n_0} v_{io}^{n_0} \quad (18)$$

over the neighboring sites i and j , instead of the strictly local definition (10). Since the diagonalization coefficients are slowly varying in space, $u_{j\sigma}^n \approx u_{i\sigma}^n$, $v_{j\sigma}^n \approx v_{i\sigma}^n$, the symmetrized $\mathcal{P}_{(ij),\sigma}$ and local $\mathcal{P}_{i,\sigma}$ Majorana polarizations are fairly similar (see Fig. 5). Some discrepancy appears at the most peripheral sites, probably due to the boundary conditions.

Let us finally recall that the complex vector $u_{i\uparrow}^{n_0} v_{i\uparrow}^{n_0}$ is typically perfectly opposite to $u_{i\downarrow}^{n_0} v_{i\downarrow}^{n_0}$ (see Fig. 3). Such antialignment implies that a modulus of the Majorana polarization can be expressed as (9) $|\mathcal{P}_i| = |\mathcal{P}_{i\uparrow} - \mathcal{P}_{i\downarrow}| = |\mathcal{P}_{i\uparrow}| + |\mathcal{P}_{i\downarrow}|$, and the same holds for the symmetrized Majorana polarization. By measuring the zero-bias conductance $\frac{dI_{ij}^\sigma(0)}{dV}$ of the spin-selective Andreev current flowing through the neighboring sites i and j one can thus evaluate the absolute value of the symmetrized Majorana polarization

$$|\mathcal{P}_{(ij)}| = \sqrt{\frac{h}{4e^2}} \sqrt{\frac{d}{dV} [I_{ij}^\uparrow(V) + I_{ij}^\downarrow(V)]}_{V=0}. \quad (19)$$

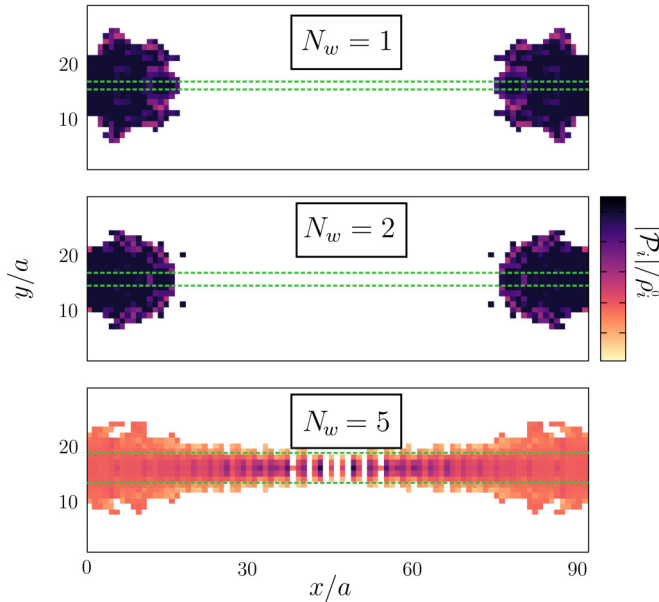


FIG. 6. The spatial profile of $|\mathcal{P}_i|/\rho_i^0$ for the potential zero-energy Majorana quasiparticles appearing in the metallic strip consisting of 1, 2, and 5 rows of atomic chains, as indicated. We have used the same model parameters as in Fig. 2: $\Delta = 0.25t$, $\phi = \pi$, $\lambda = 0.5t$, $B_0 = 0.1t$, $\mu = -3.75t$. The difference between the well-isolated MBS and the delocalized states in the wider strip is evident.

As far as the spatial variation of the phase is concerned, its determination would be evidently more cumbersome. This problem is beyond the scope of this study.

Although the spatial variation of the phase is not currently measurable, we can compare the absolute value of $|\mathcal{P}_i|$ with $\rho_i(0)$. For a MBS these must be the same, therefore, if we plot the ratio of these measurable quantities $|\mathcal{P}_i|/\rho_i(0)$, it should be flat for a MBS. In Fig. 6 we show results for $N_w \in \{1, 2, 5\}$, comparable to Fig. 2, which show that the MBS profile is indeed flat. For $N_w = 5$, when the two MBS at either end of the strip start to overlap, this quantity is no longer flat. Thus, this can be used as an experimental determination of whether localized states are actually MBS. It is worth noting that increasing the length N_x of the system would result in $|\mathcal{P}_i|/\rho_i(0)$ being flat even for $N_w > 5$.

Our Eq. (19) demonstrates analytically the feasibility of measuring a modulus of the symmetrized Majorana polarization, which we have so far illustrated for relatively small system sizes (Fig. 5). Now, we would like to verify its usefulness for probing an experimentally realistic situation. For this purpose we have used the KWANT package [47] to compute the local (10) and symmetrized (18) Majorana polarizations for the larger sample, comprising 2000×300 sites, adopting the model parameters reported in Refs. [27,28]. Figure 7 displays profiles of these polarizations obtained near a boundary of the proximitized metallic strip. It clearly shows that in realistic samples the symmetrized Majorana polarization is practically identical with the local one.

V. LOCALIZATION OF THE MAJORANA MODES

In Sec. III we have shown that upon increasing the width N_w of a metallic strip the topological superconducting state

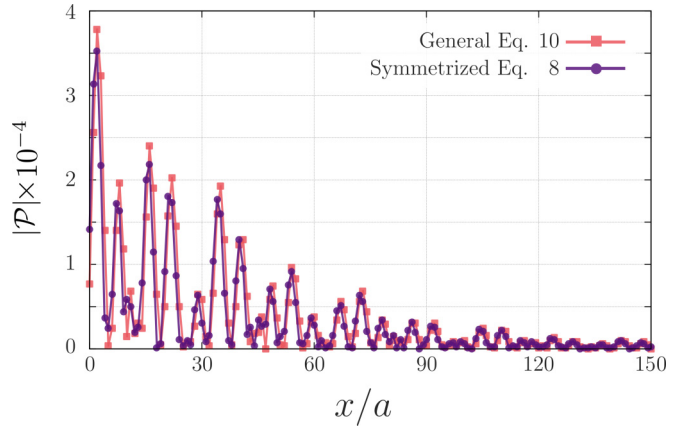


FIG. 7. Same as in Fig. 5 obtained by KWANT package for the larger size system $N_x = 2000$, $N_y = 300$, and $N_w = 5$. In analogy to Refs. [27,28] we have assumed the model parameters $t = 32$ meV, $\Delta = 0.16$ meV, $\lambda = 2.85$ meV, $B_0 = 0.12$ meV, $\mu = -120$ meV, imposing the phase difference $\phi = \pi$.

reveals (i) smearing of the Majorana quasiparticle, and (ii) development of the transverse gradient of the Majorana polarization. One may ask, however, whether there is any chance of localization of the Majorana modes. In this section we illustrate that such an effect could be observable due to local defects introduced in certain regions of the metallic strip.

Topological superconductivity in one-dimensional wires and atomic chains has been shown to be robust against weak disorder [48–55], noise [56], inhomogeneous spin-orbit coupling [57], reorientation of the magnetic field [39,58], and thermal fluctuations [59–62]. Sufficiently strong scattering centers, however, could effectively break these one-dimensional systems into separate segments, inducing additional pairs of the Majorana modes [46]. Such a mechanism can be expected to be inefficient in two-dimensional systems. To verify this conjecture for the quasi-two-dimensional heterostructure discussed in this paper we take into consideration a pointlike electrostatic defect $\mathcal{H}_{\text{imp}} = V_0 d_{i_0\sigma}^\dagger d_{i_0\sigma}$ positioned at site i_0 of the metallic region. We assume this scattering potential to be rather strong, $V_0 = 10t$, as otherwise its influence would be less visible.

Let us first assume the scattering potential to be placed in a central part of the metallic region [Fig. 8(a)]. Neither the zero-energy spectral function nor the Majorana polarization reveal any influence of such an electrostatic impurity on the existing Majorana quasiparticles, in contrast to the properties of one-dimensional topological superconductors [46]. This behavior seems to be quite natural because the Majorana modes are safely distant from the impurity.

Contrary to this situation, let us next consider the scattering potential near the left side of the metallic strip [Figs. 8(b) and 8(c)]. We selected the specific sites $i_0 = 4$ and 8 , in order to guarantee a considerable overlap of the local defect with the left-hand Majorana mode. Under such circumstances, the scattering potential has a substantial influence both on the spectral function (left panels) and the Majorana polarization (right panels). This electrostatic impurity reduces the spatial extent of the Majorana quasiparticle on the left-hand side, whereas the other Majorana quasiparticle is practically left

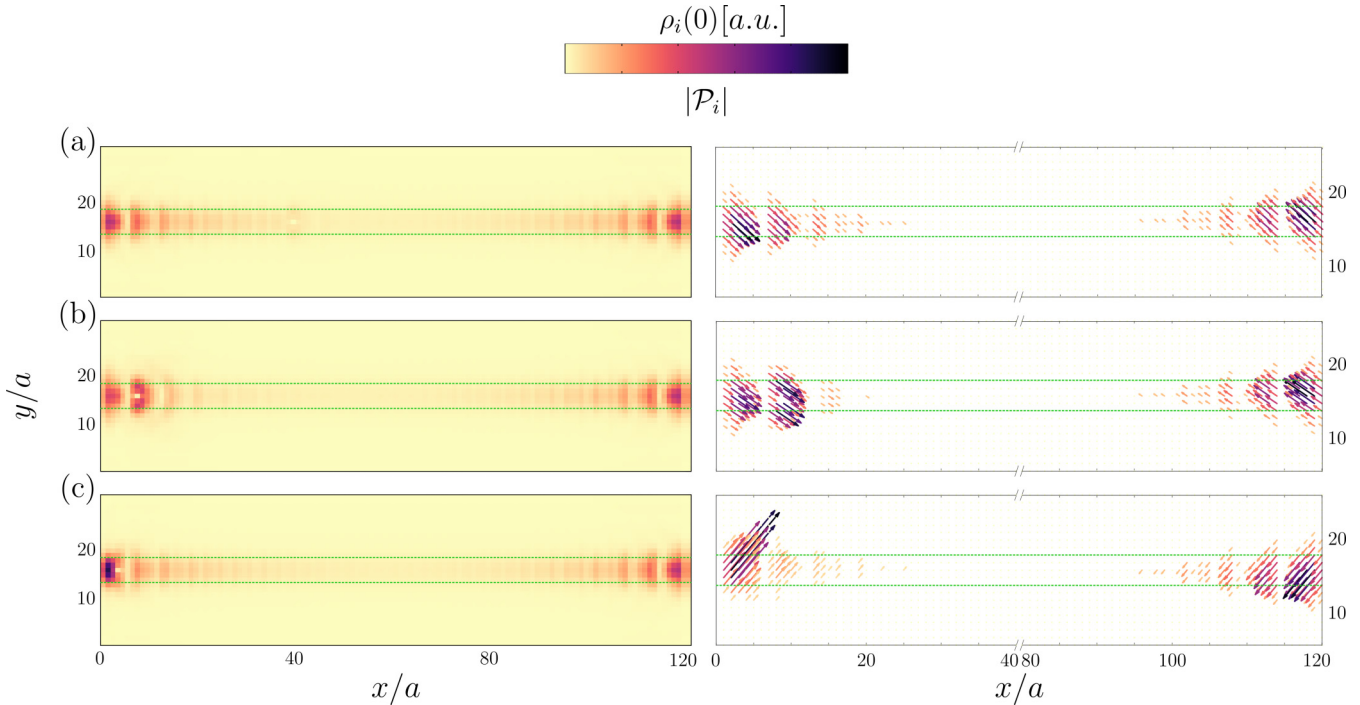


FIG. 8. The spatial density profile of the zero-energy Majorana quasiparticles (left panels) and their polarizations (right panels) obtained in the proximitized metallic strip, consisting of $N_w = 5$ rows of atoms, in presence of a pointlike electrostatic defect with $V_0 = 10t$ at site (a) $i_0 = 40a$, (b) $i_0 = 8a$, and (c) $i_0 = 4a$, with $N_x = 120$ and $N_y = 30$. The magnitude of the arrows in the right-hand-side plots show $|\mathcal{P}_{io}|$ and their directions show $\text{Arg } \mathcal{P}_{io}$. We note that the phase is only well defined up to a global shift.

intact. Such a tendency toward localization of the Majorana modes has been recently predicted by Haim and Stern [35], when investigating the different role of weak extended disorder.

Our present study provides more detailed information concerning such disorder-induced localization, indicating that (i) disorder present in the internal segments of the metallic strip would naturally be rather ineffective for the Majorana quasiparticles, whereas (ii) disorder introduced to the regions of already existing Majorana quasiparticles substantially reduces their spatial extent. The considerations discussed in Sec. IV suggest that empirical detection of this subtle phenomenon could be feasible. A tendency toward the localization of the Majorana quasiparticles could be observed in the maps of differential conductance for the spin-polarized Andreev current induced via the metallic region in the presence of the intentionally deposited local defects. Such an electrostatic scattering potential could be created by applying gate potentials, whereas a magnetic potential, leading to similar effects, can be obtained by locally perturbing the Zeeman field.

VI. SUMMARY

We have theoretically studied the properties of the Majorana quasiparticles emerging in a narrow metallic strip sandwiched between two s -wave superconductors in a Josephson-junction geometry. The topological superconducting phase has been recently reported for such metallic strips by the groups in Copenhagen [27] and Harvard [28] with a length-to-width ratio ranging from 20 to 100, respectively. Using the Bogoliubov-de Gennes treatment we have investi-

tigated the role of the finite metallic strip width, exploring its influence on (a) spatial profiles of the zero-energy quasiparticles and (b) topography of the Majorana polarization that probes the particle-hole overlap of the zero-energy quasiparticles. Furthermore, we have proposed a feasible method for detecting the magnitude of such a Majorana polarization by measuring the differential conductance in spin-polarized Andreev reflection spectroscopy.

We have also analyzed the influence of strong (pointlike) electrostatic defects on the Majorana modes. We have revealed that such a local scattering potential can affect the localization length of the Majorana quasiparticles if deposited near the ends of the metallic strip. Under such circumstances, the neighboring Majorana mode substantially reduces its spatial extent, which can be compared with what has been predicted in Ref. [35], whereas the opposite-end Majorana mode remains practically intact. Similar coexistences of the localized and delocalized Majorana quasiparticles have been previously observed by scanning tunneling spectroscopy using a disordered monolayer of superconducting Pb coupled to underlying Co-Si magnetic islands [22]. We hope that proximitized metallic strips would be a convenient platform not only for the realization of topological superconductivity, tunable by the magnetic field and Josephson phase, but could also allow for manipulating the Majorana quasiparticle length scale.

ACKNOWLEDGMENT

We thank B. Scharf for instructive discussions. This work is supported by National Science Centre (Poland) under the Grants No. UMO-2017/27/N/ST3/01762 (S.G.),

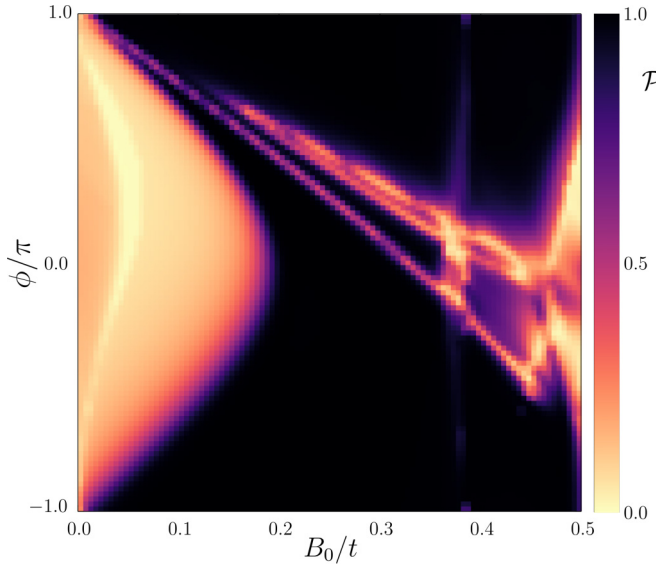


FIG. 9. The topologically nontrivial superconducting phase (dark area) with respect to the magnetic field B_0 and the Josephson phase ϕ obtained by the criterion concerning the global Majorana polarization [21,36]. Numerical computations were done for $N_w = 2$ and the same model parameters as in Fig. 2.

No. UMO-2018/29/B/ST3//01892 (N.S.), and No. UMO-2017/27/B/ST3/01911 (T.D.).

APPENDIX A: INFLUENCE OF THE JOSEPHSON PHASE

In the main part of this paper we have analyzed the spectroscopic properties of the Majorana quasiparticles, focusing on the particular case $\phi = \pi$, that is optimal for occurrence of the topological superconducting state. Similar qualitative features would be also observable for other values of the Josephson phase $\phi \neq \pi$, provided that model parameters (such as, e.g., the magnetic field) are appropriately tuned [25,26]. A possible

criterion (proposed by one of us [21,36]) for determination of the topological phase diagram relies on the Majorana polarization for MBS to be nonvanishing when summed over a portion of the investigated system where the bound states should reside, in fact it should be equal to the total density of the state in the same region. Therefore,

$$\mathcal{P} = \sum_{i \in \mathcal{R}} \frac{|\mathcal{P}_{in_0}|}{\rho_i(E_{n_0})} = 1 \quad (\text{A1})$$

for a MBS. This serves as a proxy for being in the topologically nontrivial phase. In the present scenario one can choose for this purpose either the leftmost or rightmost quarter of the metallic strip as the region \mathcal{R} . More details can be found in Ref. [21].

Figure 9 displays the topological phase diagram, with the dark area being the nontrivial phase, obtained using this criterion for our heterostructure. We show the phase diagram with respect to the magnetic field B_0 and the Josephson phase ϕ . Let us remark that such a criterion yields a smooth changeover between the topologically trivial and nontrivial superconducting states instead of a sharp transition. It can be hence useful for exploring the robustness of the topological state against perturbations such as inhomogeneity or thermal fluctuations.

APPENDIX B: LOCALIZATION BY DISORDER

Numerous studies [48–55] have shown that the topological superconductivity of one-dimensional systems is pretty stable against a weak disorder. In the phase-controlled Josephson junctions, however, Haim and Stern [35] have predicted that a weak disorder could affect topography of the Majorana modes by reducing their spatial extent. We address here briefly this intriguing effect within the Bogoliubov–de Gennes formalism. For the purpose of comparison with the results discussed in Sec. V we assume that the random scattering potential V_i is

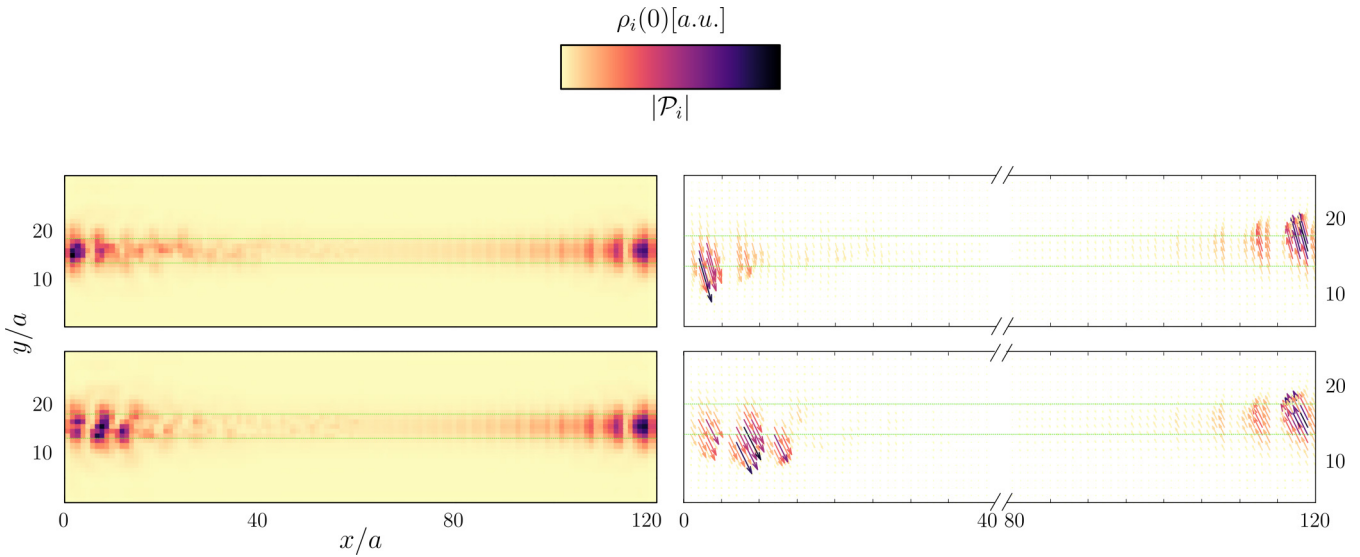


FIG. 10. The zero-energy spectral function $\rho_i(0)$ and Majorana polarization with the random scattering potential in the left half of the proximitized strip $V_i \in (-\delta V; \delta V)$ with $\delta V = 0.5t$ (top) and $\delta V = 0.75t$ (bottom). Results are obtained for the same model parameters as in Fig. 2.

present only in the left-hand side of the metallic strip, whereas the remaining (right-hand side) part is homogeneous.

Figure 10 displays topographic features of the zero-energy quasiparticles obtained for representative amplitudes δV of the random scattering potential $V_i \in (-\delta V; \delta V)$. The upper panel corresponds to $\delta V = 0.5t$ and the bottom one to $\delta V = 0.75t$, respectively. We can clearly recognize shrinking of the

Majorana quasiparticle extent in a disordered fragment of the metallic strip while in the other (homogeneous) piece the Majorana quasiparticle remains practically untouched. Such localization driven by the strong local scattering potential (Sec. V) and the weak disorder [35] seems to be unique to the topological superconducting phase in quasi-two-dimensional systems.

-
- [1] M. T. Deng, C. L. Yu, G. Y. Huang, M. Larsson, P. Caroff, and H. Q. Xu, Anomalous zero-bias conductance peak in a Nb–InSb nanowire–Nb hybrid device, *Nano Lett.* **12**, 6414 (2012).
 - [2] V. Mourik, K. Zuo, S. M. Frolov, S. R. Plissard, E. P. A. M. Bakkers, and L. P. Kouwenhoven, Signatures of Majorana fermions in hybrid superconductor-semiconductor nanowire devices, *Science* **336**, 1003 (2012).
 - [3] A. Das, Y. Ronen, Y. Most, Y. Oreg, M. Heiblum, and H. Shtrikman, Zero-bias peaks and splitting in an Al–InAs nanowire topological superconductor as a signature of Majorana fermions, *Nat. Phys.* **8**, 887 (2012).
 - [4] A. D. K. Finck, D. J. Van Harlingen, P. K. Mohseni, K. Jung, and X. Li, Anomalous Modulation of a Zero-Bias Peak in a Hybrid Nanowire-Superconductor Device, *Phys. Rev. Lett.* **110**, 126406 (2013).
 - [5] R. M. Lutchyn, E. P. A. M. Bakkers, L. P. Kouwenhoven, P. Krogstrup, C. M. Marcus, and Y. Oreg, Majorana zero modes in superconductor-semiconductor heterostructures, *Nat. Rev. Mater.* **3**, 52 (2018).
 - [6] S. Nadj-Perge, I. K. Drozdov, J. Li, H. Chen, S. Jeon, J. Seo, A. H. MacDonald, B. A. Bernevig, and A. Yazdani, Observation of Majorana fermions in ferromagnetic atomic chains on a superconductor, *Science* **346**, 602 (2014).
 - [7] R. Pawlak, M. Kisiel, J. Klinovaja, T. Meier, S. Kawai, T. Glatzel, D. Loss, and E. Meyer, Probing atomic structure and Majorana wavefunctions in mono-atomic Fe chains on superconducting Pb surface, *npj Quantum Inf.* **2**, 16035 (2016).
 - [8] B. E. Feldman, M. T. Randeria, J. Li, S. Jeon, Y. Xie, Z. Wang, I. K. Drozdov, B. A. Bernevig, and A. Yazdani, High-resolution studies of the Majorana atomic chain platform, *Nat. Phys.* **13**, 286 (2016).
 - [9] M. Ruby, B. W. Heinrich, Y. Peng, F. von Oppen, and K. J. Franke, Exploring a proximity-coupled Co chain on Pb (110) as a possible Majorana platform, *Nano Lett.* **17**, 4473 (2017).
 - [10] S. Jeon, Y. Xie, J. Li, Z. Wang, B. A. Bernevig, and A. Yazdani, Distinguishing a Majorana zero mode using spin-resolved measurements, *Science* **358**, 772 (2017).
 - [11] H. Kim, A. Palacio-Morales, T. Posske, L. Rózsa, K. Palotás, L. Szunyogh, M. Thorwart, and R. Wiesendanger, Toward tailoring Majorana bound states in artificially constructed magnetic atom chains on elemental superconductors, *Sci. Adv.* **4**, eaar5251 (2018).
 - [12] F. Nichele, A. C. C. Drachmann, A. M. Whiticar, E. C. T. O’Farrell, H. J. Suominen, A. Fornieri, T. Wang, G. C. Gardner, C. Thomas, A. T. Hatke, P. Krogstrup, M. J. Manfra, K. Flensberg, and Ch. M. Marcus, Scaling of Majorana Zero-Bias Conductance Peaks, *Phys. Rev. Lett.* **119**, 136803 (2017).
 - [13] J. Röntynen and T. Ojanen, Topological Superconductivity and High Chern Numbers in 2D Ferromagnetic Shiba Lattices, *Phys. Rev. Lett.* **114**, 236803 (2015).
 - [14] K. Björnson, S. S. Pershoguba, A. V. Balatsky, and A. M. Black-Schaffer, Spin-polarized edge currents and Majorana fermions in one- and two-dimensional topological superconductors, *Phys. Rev. B* **92**, 214501 (2015).
 - [15] J. Li, T. Neupert, Z. Wang, A. H. MacDonald, A. Yazdani, and B. A. Bernevig, Two-dimensional chiral topological superconductivity in Shiba lattices, *Nat. Commun.* **7**, 12297 (2016).
 - [16] S. Rachel, E. Mascot, S. Cocklin, M. Vojta, and D. K. Morr, Quantized charge transport in chiral Majorana edge modes, *Phys. Rev. B* **96**, 205131 (2017).
 - [17] Y. Volpez, D. Loss, and J. Klinovaja, Rashba sandwiches with topological superconducting phases, *Phys. Rev. B* **97**, 195421 (2018).
 - [18] G. C. Ménard, S. Guissart, Ch. Brun, R. T. Leriche, M. Trif, F. Debontridder, D. Demaille, D. Roditchev, P. Simon, and T. Cren, Two-dimensional topological superconductivity in Pb/Co/Si(111), *Nat. Commun.* **8**, 2040 (2017).
 - [19] Q. L. He, L. Pan, A. L. Stern, E. C. Burks, X. Che, G. Yin, J. Wang, B. Lian, Q. Zhou, E. S. Choi, K. Murata, X. Kou, Z. Chen, T. Nie, Q. Shao, Y. Fan, S.-C. Zhang, K. Liu, J. Xia, and K. L. Wang, Chiral Majorana fermion modes in a quantum anomalous Hall insulator–superconductor structure, *Science* **357**, 294 (2017).
 - [20] A. Palacio-Morales, E. Mascot, S. Cocklin, H. Kim, S. Rachel, D. K. Morr, and R. Wiesendanger, Atomic-scale interface engineering of Majorana edge modes in a 2D magnet-superconductor hybrid system, *Sci. Adv.* **5**, eaav6600 (2019).
 - [21] N. Sedlmayr, J. M. Aguiar-Hualde, and C. Bena, Majorana bound states in open quasi-one-dimensional and two-dimensional systems with transverse Rashba coupling, *Phys. Rev. B* **93**, 155425 (2016).
 - [22] G. Ménard, A. Mesaros, C. Brun, F. Debontridder, D. Roditchev, P. Simon, and T. Cren, Isolated pairs of Majorana zero modes in a disordered superconducting lead monolayer, *Nat. Commun.* **10**, 2587 (2019).
 - [23] A. Kobiałka, A. Ptak, and T. Domalski, Delocalisation of Majorana quasiparticles in plaquette-nanowire hybrid system, *Sci. Rep.* **9**, 12933 (2019).
 - [24] E. Mascot, S. Cocklin, S. Rachel, and D. K. Morr, Dimensional tuning of Majorana fermions and real space counting of the Chern number, *Phys. Rev. B* **100**, 184510 (2019).
 - [25] F. Pientka, A. Keselman, E. Berg, A. Yacoby, A. Stern, and B. I. Halperin, Topological Superconductivity in a Planar Josephson Junction, *Phys. Rev. X* **7**, 021032 (2017).
 - [26] M. Hell, M. Leijnse, and K. Flensberg, Two-Dimensional Platform for Networks of Majorana Bound States, *Phys. Rev. Lett.* **118**, 107701 (2017).
 - [27] A. Fornieri, A. M. Whiticar, F. Setiawan, E. Portoles, A. C. C. Drachmann, A. Keselman, S. Gronin, C. Thomas, T. Wang, R. Kallaher, G. C. Gardner, E. Berg, M. J. Manfra, A. Stern,

- Ch. M. Marcus, and F. Nichele, Evidence of topological superconductivity in planar Josephson junctions, *Nature (London)* **569**, 89 (2019).
- [28] H. Ren, F. Pientka, S. Hart, A. T. Pierce, M. Kosowsky, L. Lunczer, R. Schlereth, B. Scharf, E. M. Hankiewicz, L. W. Molenkamp, B. I. Halperin, and A. Yacoby, Topological superconductivity in a phase-controlled Josephson junction, *Nature (London)* **569**, 93 (2019).
- [29] W. Mayer, M. C. Dartailh, J. Yuan, A. Wickramasinghe, K. S. Matos-Abiague, I. Žutić, and J. Shabani, Phase signature of topological transition in Josephson junctions, *arXiv:1906.01179*.
- [30] F. Setiawan, C. T. Wu, and K. Levin, Full proximity treatment of topological superconductors in Josephson-junction architectures, *Phys. Rev. B* **99**, 174511 (2019).
- [31] F. Setiawan, A. Stern, and E. Berg, Topological superconductivity in planar Josephson junctions: Narrowing down to the nanowire limit, *Phys. Rev. B* **99**, 220506(R) (2019).
- [32] B. Scharf, F. Pientka, H. Ren, A. Yacoby, and E. M. Hankiewicz, Tuning topological superconductivity in phase-controlled Josephson junctions with Rashba and Dresselhaus spin-orbit coupling, *Phys. Rev. B* **99**, 214503 (2019).
- [33] T. Laeven, B. Nijholt, M. Wimmer, and A. R. Akhmerov, Enhanced proximity effect in zigzag-shaped Majorana Josephson junctions, *arXiv:1903.06168*.
- [34] A. Stern and E. Berg, Fractional Josephson Vortices and Braiding of Majorana Zero Modes in Planar Superconductor-Semiconductor Heterostructures, *Phys. Rev. Lett.* **122**, 107701 (2019).
- [35] A. Haim and A. Stern, Benefits of Weak Disorder in One-Dimensional Topological Superconductors, *Phys. Rev. Lett.* **122**, 126801 (2019).
- [36] N. Sedlmayr and C. Bena, Visualizing Majorana bound states in one and two dimensions using the generalized Majorana polarization, *Phys. Rev. B* **92**, 115115 (2015).
- [37] N. Sedlmayr, G. Guigou, P. Simon, and C. Bena, Majoranas with and without a ‘character’: Hybridization, braiding and chiral Majorana number, *J. Phys.: Condens. Matter* **27**, 455601 (2015).
- [38] M. M. Maśka and T. Domanski, Polarization of the Majorana quasiparticles in the Rashba chain, *Sci. Rep.* **7**, 16193 (2017).
- [39] V. Kaladzhyan, J. Despres, I. Mandal, and C. Bena, Majorana fermions in finite-size strips with in-plane magnetic fields, *Eur. Phys. J. B* **90**, 211 (2017).
- [40] J. J. He, T. K. Ng, P. A. Lee, and K. T. Law, Selective Equal-Spin Andreev Reflections Induced by Majorana Fermions, *Phys. Rev. Lett.* **112**, 037001 (2014).
- [41] H. H. Sun, K. W. Zhang, L. H. Hu, C. Li, G. Y. Wang, H. Y. Ma, Z. A. Xu, C. L. Gao, D. D. Guan, Y. Y. Li, C. Liu, D. Qian, Y. Zhou, L. Fu, S. C. Li, F. C. Zhang, and J. F. Jia, Majorana Zero Mode Detected with Spin Selective Andreev Reflection in the Vortex of a Topological Superconductor, *Phys. Rev. Lett.* **116**, 257003 (2016).
- [42] D. Chevallier and J. Klinovaja, Tomography of Majorana fermions with STM tips, *Phys. Rev. B* **94**, 035417 (2016).
- [43] D. Sticlet, C. Bena, and P. Simon, Spin and Majorana Polarization in Topological Superconducting Wires, *Phys. Rev. Lett.* **108**, 096802 (2012).
- [44] N. Sedlmayr, J. M. Aguiar-Hualde, and C. Bena, Flat Majorana bands in two-dimensional lattices with inhomogeneous magnetic fields: Topology and stability, *Phys. Rev. B* **91**, 115415 (2015).
- [45] A. Y. Kitaev, Unpaired Majorana fermions in quantum wires, *Phys. Usp.* **44**, 131 (2001).
- [46] M. M. Maśka, A. Gorczyca-Goraj, J. Tworzydło, and T. Domański, Majorana quasiparticles of an inhomogeneous Rashba chain, *Phys. Rev. B* **95**, 045429 (2017).
- [47] Ch. W. Groth, M. Wimmer, A. R. Akhmerov, and X. Waintal, KWANT: A software package for quantum transport, *New J. Phys.* **16**, 063065 (2014).
- [48] P. W. Brouwer, M. Duckheim, A. Romito, and F. von Oppen, Topological superconducting phases in disordered quantum wires with strong spin-orbit coupling, *Phys. Rev. B* **84**, 144526 (2011).
- [49] W. DeGottardi, D. Sen, and S. Vishveshwara, Majorana Fermions in Superconducting 1D Systems Having Periodic, Quasiperiodic, and Disordered Potentials, *Phys. Rev. Lett.* **110**, 146404 (2013).
- [50] H.-Y. Hui, J. D. Sau, and S. Das Sarma, Bulk disorder in the superconductor affects proximity-induced topological superconductivity, *Phys. Rev. B* **92**, 174512 (2015).
- [51] S. Hoffman, J. Klinovaja, and D. Loss, Topological phases of inhomogeneous superconductivity, *Phys. Rev. B* **93**, 165418 (2016).
- [52] P. Zhang and F. Nori, Majorana bound states in a disordered quantum dot chain, *New J. Phys.* **18**, 043033 (2016).
- [53] S. S. Hegde and S. Vishveshwara, Majorana wave-function oscillations, fermion parity switches, and disorder in Kitaev chains, *Phys. Rev. B* **94**, 115166 (2016).
- [54] W. S. Cole, J. D. Sau, and S. Das Sarma, Proximity effect and Majorana bound states in clean semiconductor nanowires coupled to disordered superconductors, *Phys. Rev. B* **94**, 140505(R) (2016).
- [55] B. Pekerten, A. Teker, Ö. Bozat, M. Wimmer, and İ. Adagideli, Disorder-induced topological transitions in multichannel Majorana wires, *Phys. Rev. B* **95**, 064507 (2017).
- [56] Y. Hu, Z. Cai, M. A. Baranov, and P. Zoller, Majorana fermions in noisy Kitaev wires, *Phys. Rev. B* **92**, 165118 (2015).
- [57] J. Klinovaja and D. Loss, Fermionic and Majorana bound states in hybrid nanowires with non-uniform spin-orbit interaction, *Eur. Phys. J. B* **88**, 62 (2015).
- [58] B. Kiczek and A. Ptak, Influence of the orbital effects on the Majorana quasi-particles in a nanowire, *J. Phys.: Condens. Matter* **29**, 495301 (2017).
- [59] J. Klinovaja, P. Stano, A. Yazdani, and D. Loss, Topological Superconductivity and Majorana Fermions in RKKY Systems, *Phys. Rev. Lett.* **111**, 186805 (2013).
- [60] B. Braunecker and P. Simon, Self-stabilizing temperature-driven crossover between topological and nontopological ordered phases in one-dimensional conductors, *Phys. Rev. B* **92**, 241410(R) (2015).
- [61] W. Hu, R. T. Scalettar, and R. R. P. Singh, Interplay of magnetic order, pairing, and phase separation in a one-dimensional spin-fermion model, *Phys. Rev. B* **92**, 115133 (2015).
- [62] A. Gorczyca-Goraj, T. Domański, and M. M. Maśka, Topological superconductivity at finite temperatures in proximitized magnetic nanowires, *Phys. Rev. B* **99**, 235430 (2019).